

# In situ synthesis and electrophoretic deposition of CNT–ZnS:Mn luminescent nanocomposites

Alireza Naeimi · Amir Masoud Arabi ·  
Mahdi Shafiee Afarani · Amir Reza Gardeshzadeh

Received: 15 September 2014 / Accepted: 25 November 2014 / Published online: 30 November 2014  
© Springer Science+Business Media New York 2014

**Abstract** Intertwined composites of carbon nanotubes (CNTs)–manganese doped zinc sulfide (ZnS:Mn) was prepared by precipitating ZnS:Mn nanoparticles on the CNTs surface followed by electrophoretic deposition on Al substrates. Proper distribution of zinc sulfide nanoparticles on the CNTs surface was obtained via its surface modification by polyvinylpyrrolidone (PVP) and ethylene glycol (EG). The results revealed that cubic zinc sulfide was formed in the deposited nanocomposites. Transmission electron microscope (TEM) showed deagglomeration of ZnS nanoparticles on the CNTs surface in the presence of EG and PVP. Moreover, electrophoretic (EPD) characteristics (i.e. weight deposition, current density and deposition rate) and photoluminescence (PL) measurements confirmed the significant effect of EG and PVP on different properties of CNT–ZnS:Mn nanocomposites. Optimum concentration of PVP was 25 wt% of CNTs, while 50 ml EG showed better EPD and PL properties. The sample containing 25 wt% PVP represented the best coating quality but the highest PL intensities were obtained for the sample synthesized in the presence of 40 ml EG.

## 1 Introduction

In recent years, many researches have been focused on synthesis and application of carbon nanotubes (CNTs) [1, 2]. CNTs nanocomposites are one of major approaches for making use of dispersed carbon nanotubes [3]. Carbon nanotube composites have different types including CNT–polymers, CNT–metals and CNT–ceramics [3–5]. Increased stiffness, strength, and toughness are the main reasons of introducing CNTs to polymer or ceramic (such as alumina, zirconia and silicon carbide) matrices [6–10]. CNT–ceramic composites such as ZnS–CNT [11] and TiO<sub>2</sub>–CNT [12, 13] for photo-catalytic applications, MnO<sub>2</sub>–CNT [14, 15] and SnO<sub>2</sub>–CNT [16] sensors, or ZnS:Cu–CNT [17] and LiO<sub>4</sub>:Eu–CNT [18] field emission devices are some instances. CNT nanocomposites preparation needs CNTs to be well dispersed through functionalization by different surfactants.

In recent decades, different methods and agents have been reported for functionalization of CNTs [19]. They can be well dispersed in water using either anionic, cationic, or nonionic surfactants such as sodium dodecyl sulfate (SDS) and sodium dodecylbenzene sulfonate (SDBS), cetyltrimethylammonium bromide (CTAB), Brij, Tween, Triton X, and siloxane polyether copolymer (PSPEO) [20]. In addition, non-covalent interactions with different groups have been utilized to generate water dispersible CNTs [21]. Polyvinyl pyrrolidone (PVP), polyvinyl alcohol (PVA) and polyethyleneglycol (PEG) suppress the agglomeration of CNTs during preparation of the nanocomposite [22].

There are two methods for production of ceramic composites: (1) discrete preparation of components and then, formation of composite in the final stage; (2) in situ synthesis of at least one component in the presence of the others [23].

---

A. Naeimi · M. Shafiee Afarani (✉)  
Department of Materials Engineering, Faculty of Engineering,  
University of Sistan and Baluchestan, Zahedan, Iran  
e-mail: shafiee@eng.usb.ac.ir

A. Naeimi  
e-mail: Alireza.naeimi68@gmail.com

A. M. Arabi · A. R. Gardeshzadeh  
Department of Nanomaterials and Nanocoatings, Institute for  
Color Science and Technology (ICST), Tehran, Iran  
e-mail: aarabi@icrc.ac.ir

A. R. Gardeshzadeh  
e-mail: agardeshzadeh@icrc.ac.ir

On the other hand, for some applications such as sensors [24], electronics [25, 26] or displays [27, 28], ceramic–CNTs composites must be coated on a suitable substrate. For this purpose, electrophoretic deposition (EPD) is a promising coating method which relies on migration and deposition of charged particles (or CNTs) in a liquid suspension onto an oppositely charged electrode upon application of an external electric field [29–31]. EPD can be used for a great variety of materials such as: ceramics, metals, polymers and glasses. Moreover, the technique enables particulate materials of different size, shape and density to deposit simultaneously in order to generate uniform composite coatings of novel compositions [32, 33].

Electrophoretic deposition process for preparation of ZnS:Ag/CNTs nanocomposites on the surface of Al substrates as a novel luminescent composite was reported earlier [34]. In this work, we used nanosized ZnS:Mn particles decorated on the CNTs surface for the preparation of a new luminescent composite. Because of a high agglomeration tendency of nanosized particles, PVP and EG were added to optimize the dispersion of composites, improve the EPD process and increase the PL intensity of CNT–ZnS:Mn luminescent nanocomposites.

## 2 Experimental procedure

All chemicals were of analytical grade. Multiwalled carbon nanotubes (PL-MCNP, outer diameter of 5–20 nm, inner diameter of 2–6 nm, length of 1–10  $\mu\text{m}$ , purity >95 %) were purchased from Plasmachem GmbH company. Sodium sulfide hydrate ( $\text{Na}_2\text{S}\cdot x\text{H}_2\text{O}$ , Acros Organics), Zinc acetate [ $(\text{CH}_3\text{COO})_2\text{Zn}\cdot 2\text{H}_2\text{O}$ , MERCK] and manganese acetate [ $\text{Mn}(\text{CH}_3\text{COO})_2\cdot 4\text{H}_2\text{O}$ , MERCK] were used for synthesis of ZnS:Mn nanoparticles. Polyvinylpyrrolidone (PVP, 25, Rahavard Darou) and ethylene glycol (EG,  $\text{C}_2\text{H}_6\text{O}_2$ , MERCK) were used as surface modifiers. Moreover, magnesium nitrate hexahydrate [ $\text{Mg}(\text{NO}_3)_2\cdot 6\text{H}_2\text{O}$ , MERCK] was used for increasing the CNTs surface charge.

Because of quenching effect of carbon structures under UV light, the optimum concentration of CNTs was fixed at 10 wt% based on the PL intensities of primary experiments. The following procedure was used for synthesis of CNT–ZnS:Mn nanocomposites: First, CNT was dispersed in a nonaqueous medium. Stable suspensions of CNTs were prepared by dispersing 25, 50, 75 and 100 mg CNT powder in 100 ml absolute ethanol under ultrasonication for 10 min. All surface modifiers such as EG and PVP were added to the CNTs suspensions in this step to make the surface of CNTs ready for absorption of favorite ions. Two approaches were considered to determine the amount of surface modifiers: (1) fixing the surface modifier to CNTs

ratio in the range of 0–4, and (2) evaluating the suspension stability. The amount of PVP (0–4 wt% of CNTs) was calculated according to the first approach, while EG amount (10–80 ml) was weighted with respect to the second one. Then, 0.4 g sodium sulfide hydrate was added to the suspension during mixing (suspension A). In the second step, the cationic solution was prepared by dissolution of 1.124 g zinc acetate and 8.63 ml manganese acetate solution (0.04 g/l) in 100 ml deionized water (solution B). In the third step, Solution B was added dropwise to suspension A for 30 min. The primary composites were dried in an electric oven at 60  $^\circ\text{C}$  for 24 h and used for EPD without further purification. Reference ZnS:Mn nanoparticles were synthesized separately to compare their coating behavior with that of the nanocomposite.

For EPD process, the commercial aluminium foils (10 mm  $\times$  30 mm) used as electrode were first cleaned with acetone in an ultrasonic cleaner for 5 min and then dried at 50  $^\circ\text{C}$ . Then, 0.05 g CNT–ZnS:Mn primary nanocomposite powder was dissolved in 50 ml absolute ethanol under ultrasonication for 10 min. DC electrophoretic deposition was performed by applying voltages up to 300 V for 10 min. Coated substrates (electrodes) were gradually oven-dried at 50  $^\circ\text{C}$ .

Microstructure of the samples was analysed using scanning electron microscope (SEM, LEO 1445 VP) and transmission electron microscope (TEM, Philips Em208). XRD (Siemens D500) was used for structural characterization of obtained samples. Photoluminescence (PL) spectra were drawn using Perkin-Elmer LS 55 Luminescence Spectrometer using exciting wavelength of 360 nm. The Perkin-Elmer Spectrum One FTIR Spectrometer was used for the study of chemical compositions.

## 3 Results and discussion

### 3.1 Structural studies

The phase variation of the samples was analysed from synthesis to deposition. Figure 1 shows the X-ray diffraction pattern of CNT–ZnS:Mn nanocomposites deposited on the aluminium substrate. Major phase belongs to the aluminium substrate (Card No.: 00-001-1179). Other peaks relate to the sphalerite structure of ZnS:Mn (Card No.: 00-001-0792). Broadening of sphalerite peaks is due to the nanocrystalline nature of synthesized ZnS:Mn. Because of stronger diffraction pattern of aluminium substrate, the sphalerite phase is detected as a minor phase [35, 36]. The appearance of the peaks around 22 and 40 $^\circ$  may be assigned to the graphite structure [35, 36]. Moreover, the shift of graphite peaks to the lower 2 $\theta$  values may be due to the existence of metals in the graphene layers [37, 38].

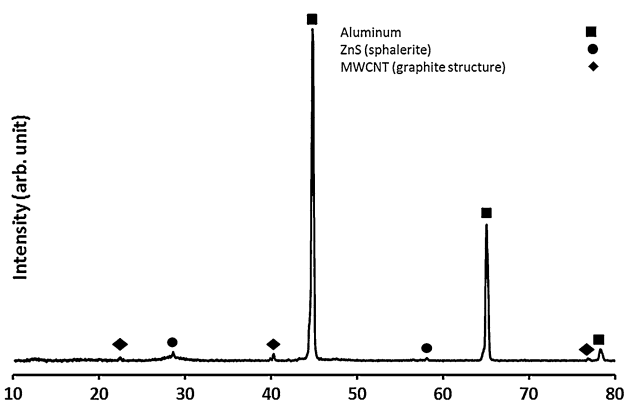


**Fig. 1** X-ray diffraction pattern of CNT–ZnS:Mn composite

### 3.2 Chemical compositions

FTIR spectra of three CNT–ZnS:Mn samples (unmodified, PVP-modified and EG-modified) are shown in Fig. 2. In the unmodified sample, two main peaks can be assigned to the stretching ( $3,400\text{ cm}^{-1}$ ) and bending ( $1,630\text{ cm}^{-1}$ ) bands of water. The weak band at  $2,373.7\text{ cm}^{-1}$  is associated with carbon and oxygen vibrations. The bands at  $1,200$  and  $1,100\text{ cm}^{-1}$  are attributed to Mn in ZnS structure. The bands at  $669, 664, 650$  and  $621\text{ cm}^{-1}$  are associated with Zn–S vibrations. The main peak located in the range of  $400\text{--}450\text{ cm}^{-1}$  is associated with ZnS structure and its bonds. Addition of PVP and EG modifiers considerably shifts the peaks and changes their shape. The presence of PVP was confirmed by the appearance of broad peaks in the range of  $1,250\text{--}1,650\text{ cm}^{-1}$  attributed to C–N and C=O bonds of PVP compound. Sharp bands located at  $2,876$  and  $1,409\text{ cm}^{-1}$  are associated to C–H bond of PVP. Moreover, weak peak of EG located around  $1,090\text{ cm}^{-1}$  belongs to C–O bonds of  $\text{CH}_2\text{-OH}$  [22, 39, 40].

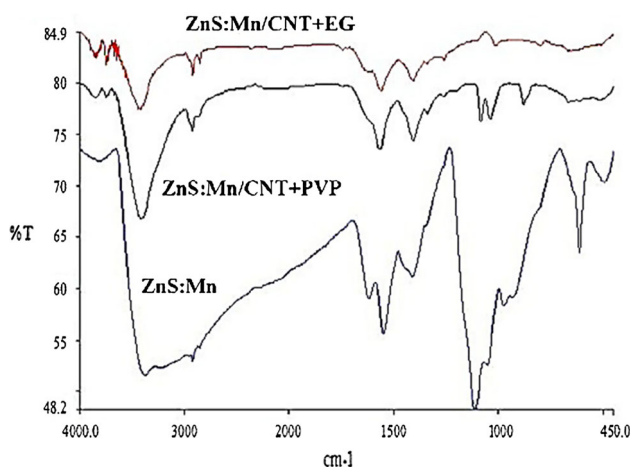


**Fig. 2** FTIR spectra for CNT–ZnS:Mn samples synthesized with EG and PVP or bare of surface modifiers

### 3.3 Electrophoretic characteristics

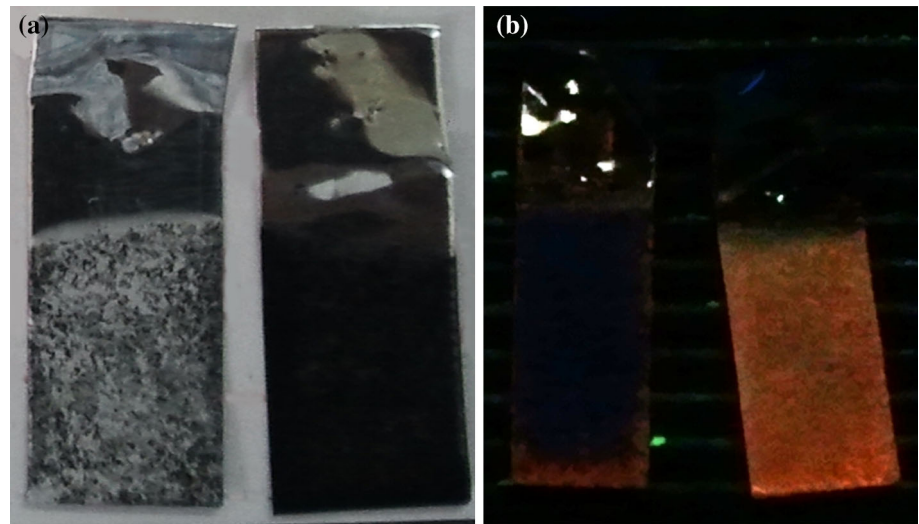
As reported earlier [34], positive charge of CNT in ethanol results in cathodic deposition (i.e. deposition on the cathode electrode). The first step in the synthesis of CNT-ZnS:Mn nanocomposites via EPD process was to determine the ZnS:Mn net charge; ZnS:Mn nanoparticles were deposited under  $300\text{ V}$  for  $2\text{ min}$  in ethanol. Results show that ZnS:Mn nanoparticles possess negative charge and the deposit has undesirably poor quality which is mainly due to the weak surface charge of ZnS nanoparticles. Thus, their surface charge was enhanced by addition of  $\text{Mg}(\text{NO}_3)_2 \cdot 6\text{H}_2\text{O}$ , resulting in the adsorption of  $\text{Mg}^{2+}$  ions on the ZnS:Mn nanoparticles (the same charge as CNTs). After adjusting the surface charge of the ZnS:Mn nanoparticles, cathodic co-depositing of CNT and ZnS:Mn was carried out.

Because of the rapid separation of CNTs and ZnS:Mn nanoparticles during EPD process (as shown in Figs. 3, 4) which was due to the formation of agglomerated ZnS:Mn nanoparticles and so ineffective charging of nanoparticles by  $\text{Mg}^{2+}$ , the in situ *synthesis* of ZnS:Mn nanoparticles in the presence of CNTs with subsequent EPD of obtained nanocomposites was carried out. The prepared nanocomposite was suitably coated on the cathode, however no PL radiation was observed. This phenomenon can be related to the undesired distribution of ZnS:Mn nanoparticles on the CNTs surface. This inhomogeneity led to the decrease of effective adsorption of photons by the nanoparticles under UV light. In the other words, most of the photons are adsorbed by CNTs rather than the luminescent nanoparticles (i.e. quenching of PL intensity). To solve the problem, addition of surface modifiers such as PVP and EG was suggested.



**Fig. 3** Separation of suspension during the EPD process of CNTs and ZnS:Mn nanoparticles

**Fig. 4** Inhomogeneous deposition of CNT and ZnS:Mn nanoparticles on two different electrodes at: **a** as deposited and **b** under UV light exposure (360 nm)



### 3.3.1 EPD of CNT–ZnS:Mn in the presence of PVP as a surface modifier

Figure 5 shows the deposition yield ( $\text{g}/\text{cm}^2$ ) of composites on the aluminium substrates as a function of PVP:CNT weight ratio. The diagram confirms that the deposition yield decreases with increasing the PVP:CNT weight ratios which may be due to the stability of CNT–ZnS:Mn composites. Macro-images of the samples are shown in Fig. 6. The best coverage of the surface with polymeric chain can be optimized at certain PVP:CNT weight ratios. At this value, the steric repulsion increases the stability and hence improves the EPD process [40, 41]. It can be concluded from Figs. 5 and 6 that the improved stability (25 wt% PVP with respect to CNTs weight) leads to higher deposition yields.

Figure 7 shows current density versus time for different PVP:CNT weight ratios. In the initial times, higher concentration of CNT–ZnS:Mn particles leads to migration of

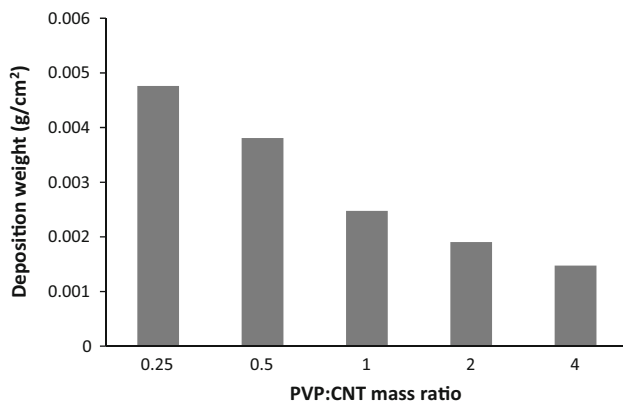


**Fig. 5** Deposition yield of CNT–ZnS:Mn composites as a function of PVP:CNT weight ratios



**Fig. 6** Macro image of CNT–ZnS:Mn suspensions with different PVP:CNT weight ratios **a** 0.25 and **b** 4

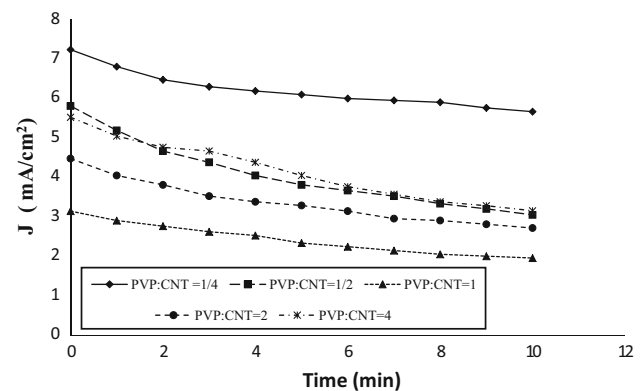


**Fig. 7** Current density of CNT–ZnS:Mn composites as a function of PVP:CNT weight ratios

more charged particles and a thicker layer of composite deposits on the electrode. So, the electrical conductivity of the electrode experiences a sudden decrease. Thereafter, the decrease of CNT–ZnS:Mn concentration in the



suspension resulted in lower electrical conductivity of the deposit and consequently, gradual change of current density with the time. Moreover, PVP:CNT weight ratios have a considerable effect on the current density. Initially, the current density decreases by increasing the weight ratio up to 1, above which a reverse behavior was observed. It is suggested that two competitive mechanisms occur with increasing the PVP:CNT ratio: (1) reduction of the suspension stability as mentioned before, (2) increase of electric conductivity due to the concentrated polymeric chains in the media [40, 41]. Therefore, there is an optimum point for PVP:CNT weight ratio (1:1) at which the minimum current density versus time is obtained.

As shown in Fig. 8, the quality of the deposited nanocomposites was also affected by the PVP:CNT weight ratios, i.e. it improves at lower ratios. The best quality was obtained for PVP:CNT ratio of 0.25 which was in good agreement with the deposition yield diagrams (Fig. 5).

### 3.3.2 EPD of CNT–ZnS:Mn in the presence of EG as a surface modifier

Ethylene Glycol was also used for surface modifying of CNT–ZnS:Mn nanocomposites, but its influence was completely different from PVP. Because of simultaneous

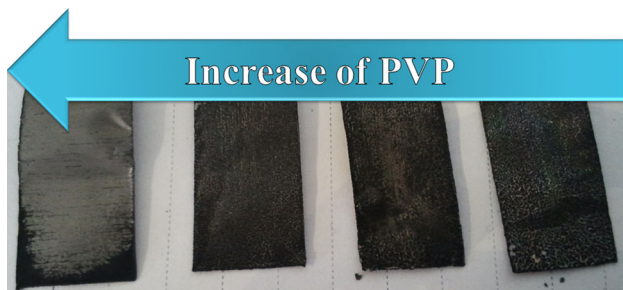


Fig. 8 Macro image of CNT–ZnS:Mn nanocomposites deposited in the presence of different PVP values

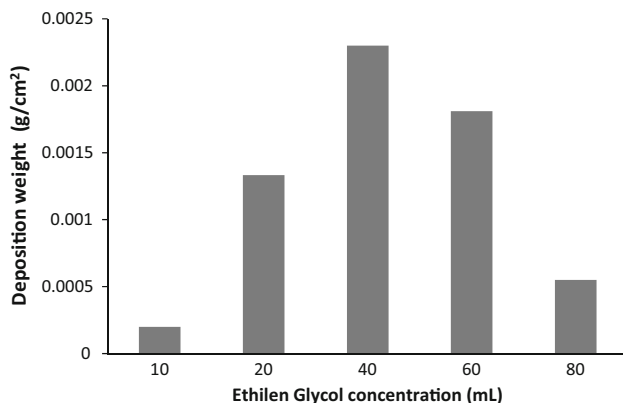


Fig. 9 Deposition yield curves of CNT–ZnS:Mn nanocomposites versus different EG concentration

solvent and capping effects of EG [35], it is more effective than PVP. So, its concentration was considered in the range of 10–50 ml. Figure 9 shows the deposition yield of CNT–

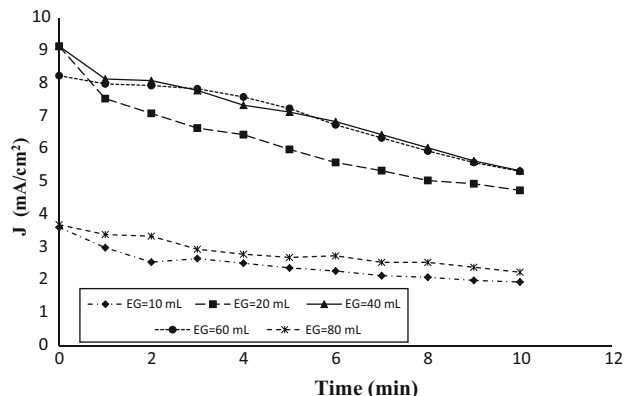


Fig. 10 Current density curves of CNT–ZnS:Mn nanocomposites versus EG concentration

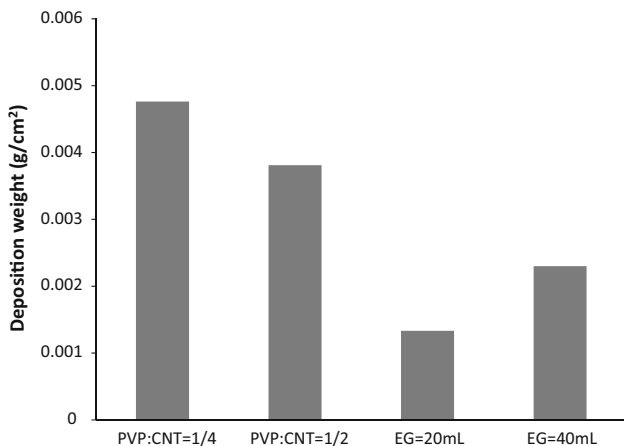


Fig. 11 The comparison of deposition yield for CNT–ZnS:Mn deposition in the presence of 0.25 and 0.5 PVP:CNT weight ratios or 20 and 40 ml of EG

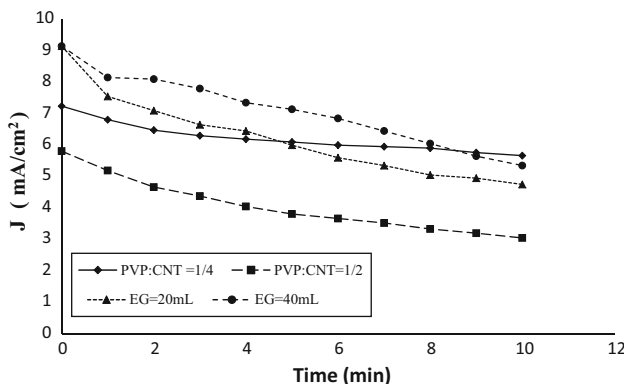
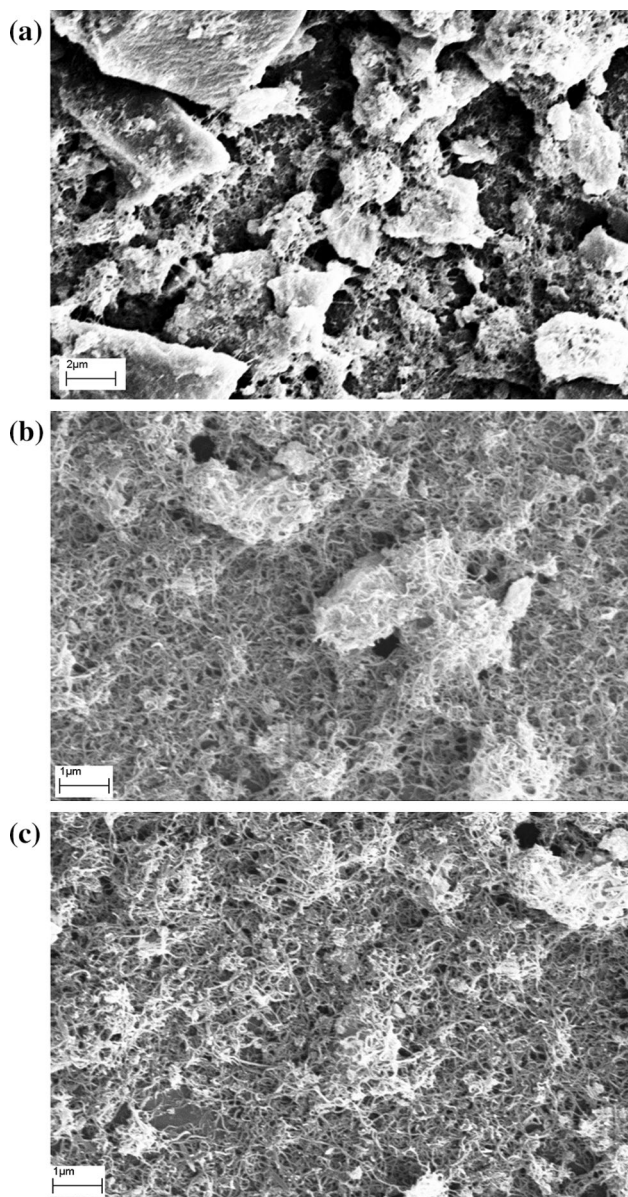


Fig. 12 The comparison of current densities for deposition of CNT–ZnS:Mn in the presence of 0.25 and 0.5 PVP:CNT weight ratios or 20 and 40 ml of EG

ZnS:Mn nanocomposites as a function of EG concentration. As illustrated in the figure, maximum deposition yield belonged to the CNT–ZnS:Mn sample synthesized in the presence of 40 ml EG. Similar trend was also observed for current densities versus time (Fig. 10). It is suggested that the effect of EG concentration on the viscosity as well as its capping and surface modifying roles lead to the optimum point of deagglomeration in nanocomposites at 40 ml. At higher EG concentrations, nanocomposites start to flocculate. Furthermore, the highest current density at 40 ml EG verifies the surface charge increasing, electrostatic stabilization and consequently successful EPD process.



**Fig. 13** SEM micrographs of CNT–ZnS:Mn nanocomposites deposited on the aluminium substrates **a** without surface modifier, **b** with PVP and **c** with EG

Formation of a non-conductive layer on the CNTs surface at EG concentrations above 40 ml suppresses current density values.

Electrophoretic deposition process for deposition of CNT–ZnS:Mn nanocomposites in the presence of PVP and EG are illustrated in Figs. 11 and 12. It seems that PVP yields more successful EPD process than EG. It may be related to higher dielectric constant ( $\epsilon_{\text{solvent}}$ ) of mixed ethanol–EG in comparison with the pure ethanol [35, 41, 42]. Based on the Hamaker's law, the mobility of charged particles increases with  $\epsilon_{\text{solvent}}$  [42–45]. So, the high velocity of particles towards the cathode leads to the formation of a dense insulator layer on the electrode in the initial stage of deposition. As a result, the deposition trend dramatically decreases and a non-uniform layer is obtained. The lower deposition yield and the higher current densities in the case of EG confirm the above mechanism.

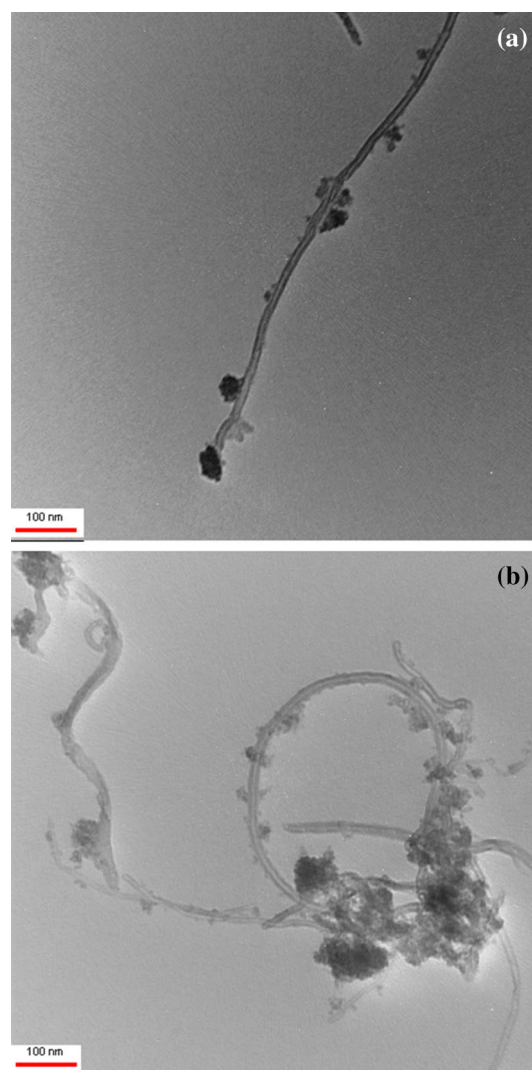


**Fig. 14** TEM micrographs of CNT–ZnS:Mn nanocomposites synthesized in the presence of **a** PVP and **b** EG

### 3.4 Microstructural studies

Figure 13 shows the SEM micrographs of CNT–ZnS:Mn samples deposited on the aluminium electrode in the presence of (a) 25 wt% PVP and (b) 40 ml EG. Although the surface modifiers improved the deposition homogeneity but some agglomerated areas are observed in both samples. It can be related to the intense agglomeration during the synthesis process or lack of proper distribution of surface modifiers around the CNT surfaces due to higher surface area in nanoscale. However, macro features of the deposition are superior in the presence of EG.

Both micrographs in Fig. 14 show that some discrete ZnS particles are formed on the surface of CNTs. However, some agglomerates are observed between the CNTs. Formation of both particulate and agglomerated features are obvious in the case of EG. It can be concluded from SEM and TEM micrographs that the surface modifiers have three distinctive roles in the formation of CNT–ZnS:Mn nanocomposites: (1) deagglomeration of CNTs, (2) deagglomeration of ZnS:Mn nanoparticles during synthesis through covering the CNTs surface and increasing the repulsion between nanoparticles and, (3) improving the EPD

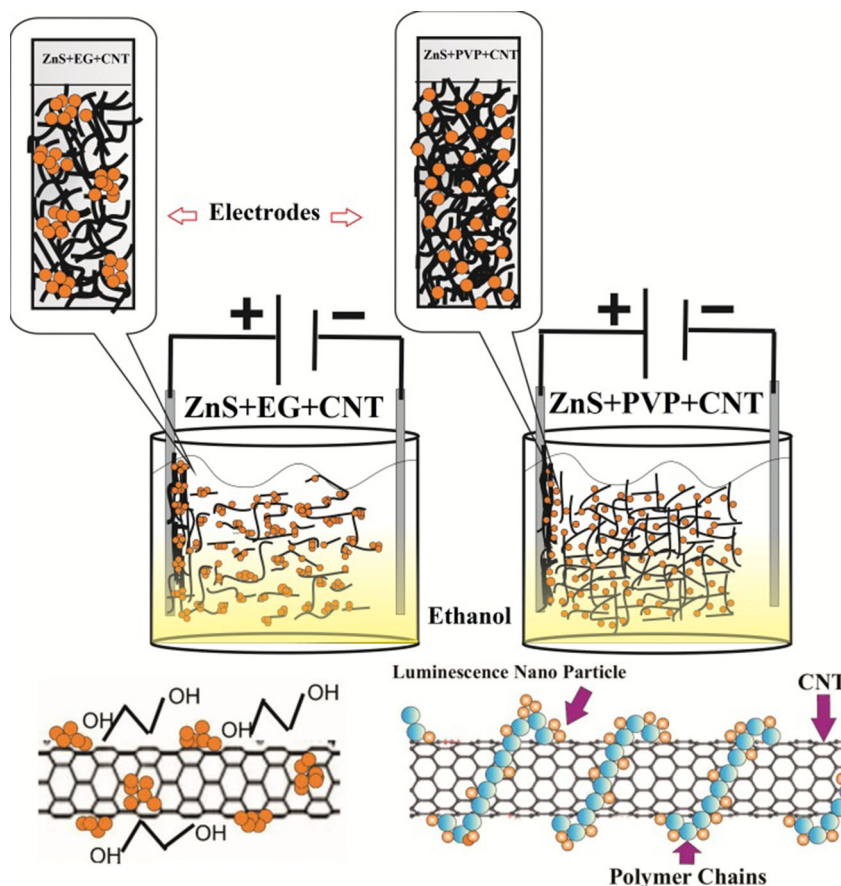
characteristics. Schematic representation of these three mechanisms is shown in Fig. 15.

It is suggested that PVP can affect the second and the third mechanisms while the first one is more sensitive to EG. It has been reported that the functionalized CNTs with EG have better distribution in aqueous media [43–46].

### 3.5 Photoluminescence properties

Primary studies of luminescence properties showed that unmodified CNT–ZnS:Mn nanocomposites could not be excited under the exposure of UV light. It was not only due to the strong agglomeration of ZnS:Mn nanoparticles on the CNTs surface, but the adsorption of UV light by CNTs carbon structure [47]. However, surface modifying of nanocomposites led to emission of light in the orange–red region of visible spectrum. Photoluminescence (PL) spectra of CNT–ZnS:Mn nanocomposites in the presence of different PVP:CNT ratios are illustrated in Fig. 16. PL spectra consist of a sharp peak with a maximum at 590 nm. This emission is due to the recombination of electron–hole which is highly activated by Mn<sup>2+</sup> diffusion in ZnS network. The peak intensities of all samples were dramatically

**Fig. 15** Schematic representation of EPD process of CNT–ZnS:Mn nanocomposites in the presence of PVP and EG as surface modifiers





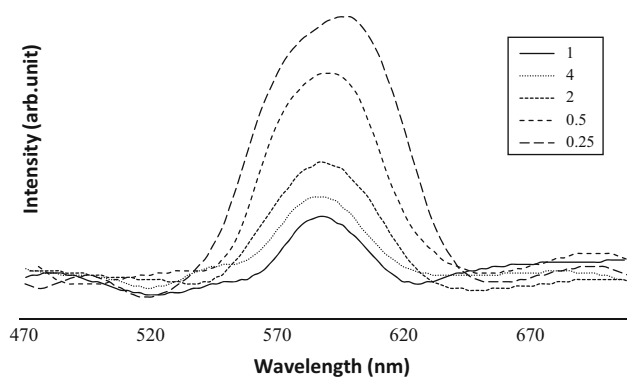


**Fig. 16** PL spectra of CNT–ZnS:Mn nanocomposites synthesized in the presence of different PVP:CNT weight ratios (0.25–4)

low. The emission phenomenon in the ZnS:Mn nanoparticles depends on the generation of two electron–hole pairs during the excitation of cubic zinc sulfide under the exposure of 330 nm UV light, but the existence of competitive path for the transformation of electrons into the CNT channels instead of relaxation causes quenching of PL intensities. However, the improvement of PL intensity at PVP:CNT weight ratio of 0.25 confirms direct relation between the surface modification and PL intensities. With increasing PVP:CNT weight ratios up to 1, suspension stability decreased and the nanocomposite agglomeration increased, leading to PL quenching. Due to the weakening of PL spectra above 0.5 weight ratios, maximum peak intensities cannot obey the regular law.

PL spectra of CNT–ZnS:Mn nanocomposites modified by different EG concentrations are shown in Fig. 17. As it is expected, there is a maximum PL intensity corresponding to more stable suspension and proper attachment of ZnS:Mn nanoparticles to CNTs. Unlike the PVP, the maximum emission intensity was not appeared for the most stable suspension. It can be related to other properties of EG such as capping [46, 48] or solvent effects [48] which

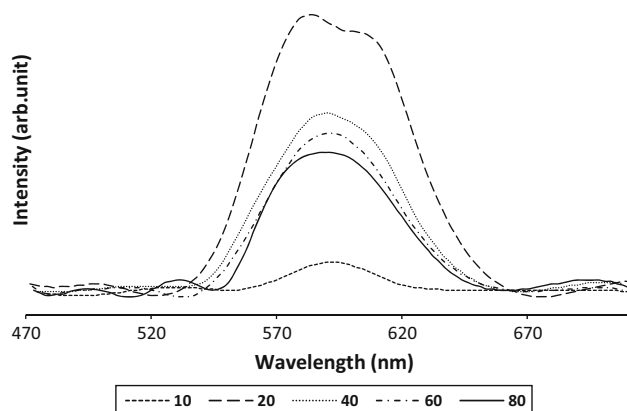


**Fig. 17** PL spectra of CNT–ZnS:Mn nanocomposites synthesized in the presence of different EG concentrations (10–80 ml)

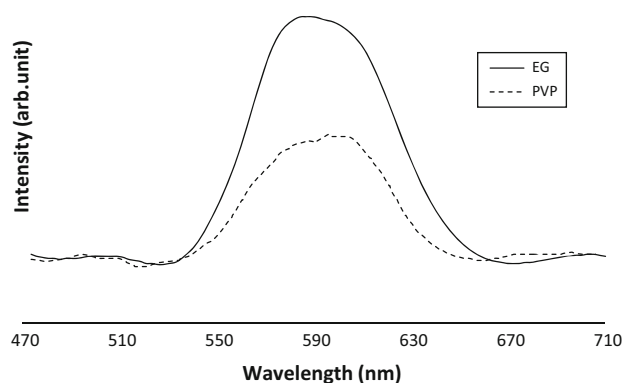


**Fig. 18** Comparison of PL spectra of optimum CNT–ZnS:Mn samples in the presence of EG and PVP

can influence the PL intensities. As shown in Fig. 18, consistency of stability with other properties of EG is the main reason for introducing the CNT–ZnS:Mn sample synthesized in the presence of 40 ml EG as the best luminescent nanocomposite. Because of a high interaction between CNT electron emitters with ZnS:Mn luminescent particles, this nanocomposite can be applicable for modern display technologies such as field emission displays (FED).

#### 4 Conclusions

The present work focused on the preparation of ZnS:Mn nanoparticle–CNT composites for luminescent applications. The results generally showed that the synthesis of ZnS:Mn nanoparticles in the presence of CNTs and then depositing by EPD method is an effective mean for preparation of ZnS:Mn/CNT nanocomposites. Addition of PVP and EG surface modifiers in the synthesis step leads to appropriate distribution of primary ZnS:Mn particles and uniform distribution of nanocomposite components. The best modification was achieved either by addition of 0.25 wt% PVP (weight ratio to CNT) or 40 ml EG to the aqueous medium before formation of ZnS:Mn nanoparticles. EPD results showed that the maximum deposition yield, current density and PL emission was attained for the optimum concentrations of surface modifiers. Moreover, more uniform deposits were obtained for PVP-containing samples, while the highest PL intensities were observed in the presence of 40 ml EG.

#### References

1. X. Liang, Transition from tubes to sheets—a comparison of the properties and applications of carbon nanotubes and graphene, in *Nanotube Superfiber Materials Changing Engineering Design*,



- ed. by M.J. Schulz, V.N. Shanov, Z. Yin (William Andrew, Elsevier, Amsterdam, 2014), pp. 519–568
2. O. Gohardani, M.C. Elola, C. Elizetxea, Potential and prospective implementation of carbon nanotubes on next generation aircraft and space vehicles: a review of current and expected applications in aerospace sciences. *Prog. Aerosp. Sci.* **70**, 42–68 (2014)
  3. S. Rul, F. Lefevre-schlick, E. Capria, C. Laurent, A. Peigney, Percolation of single-walled carbon nanotubes in ceramic matrix nanocomposites. *Acta Mater.* **52**, 1061–1067 (2004)
  4. X.-M. Liu, Z.D. Huang, W.S. Oh, B. Zhang, P.-C. Ma, M.M.F. Yuen, J.-K. Kim, Carbon nanotube (CNT)-based composites as electrode material for rechargeable Li-ion batteries: a review. *Compos. Sci. Technol.* **72**, 121–144 (2012)
  5. B.A. Rozenberga, R. Tenne, Polymer-assisted fabrication of nanoparticles and nanocomposites. *Prog. Polym. Sci.* **33**, 40–112 (2008)
  6. Z. Chen, X.J. Dai, K. Magniez, P.R. Lamb, B.L. Fox, X. Wang, Improving the mechanical properties of multiwalled carbon nanotube/epoxy nanocomposites using polymerization in a stirring plasma system. *Compos. Part A. Appl. Sci. Manuf.* **56**, 172–180 (2014)
  7. L. Bokobza, Multiwall carbon nanotube elastomeric composites: a review. *Polymer* **48**, 4907–4920 (2007)
  8. J. Echeberria, N. Rodríguez, J. Vleugels, K. Vanmeensel, A. Reyes-Rojas, A. Garcia-Reyes, C.D. Niguez-Rios, A.A. Elguézabal, M.H. Bocanegra-Bernal, Hard and tough carbon nanotube-reinforced zirconia-toughened alumina composites prepared by spark plasma sintering. *Carbon* **50**, 706–717 (2012)
  9. M. Michálek, J. Sedláček, M. Parchoviansky, M. Michálková, D. Galusek, Mechanical properties and electrical conductivity of alumina. *Ceram. Int.* **40**, 1289–1295 (2014)
  10. H.-Z. Wang, X.-D. Li, J. Ma, G.-Y. Li, T.-J. Hu, Multi-walled carbon nanotube-reinforced silicon carbide fibers prepared by polymer-derived ceramic route. *Compos. Part A. Appl. Sci. Manuf.* **43**, 317–324 (2012)
  11. L. Zhao, L. Gao, Coating multi-walled carbon nanotubes with zinc sulfide. *J. Mater. Chem.* **14**, 1001–1004 (2004)
  12. S.M. Mirandaa, G.E. Romanos, V. Likodimos, R.R.N. Marques, E.P. Favvas, F.K. Katsaros, K.L. Stefanopoulos, V.J.P. Vilarb, J.L. Faria, P. Falaras, A.M.T. Silva, Pore structure, interface properties and photocatalytic efficiency of hydration/dehydration derived TiO<sub>2</sub>/CNT composites. *Appl. Catal. B. Environ.* **147**, 65–81 (2014)
  13. M.-L. Chen, F.J. Zhang, W.C. Oh, Synthesis, characterization, and photocatalytic analysis of CNT/TiO<sub>2</sub> composites derived from MWCNTs and titanium sources. *Carbon N. Y.* **47**, 2943 (2009)
  14. M.-M. Zou, D.-J. Ai, K.-Y. Liu, Template synthesis of MnO<sub>2</sub>/CNT nanocomposite and its application in rechargeable lithium batteries. *Trans. Nonferrous Met. Soc. China* **21**, 2010–2014 (2011)
  15. F. Teng, S. Santhanagopalan, D.D. Meng, Microstructure control of MnO<sub>2</sub>/CNT hybrids under in situ hydrothermal conditions. *Solid State Sci.* **12**, 1677–1682 (2010)
  16. R.-J. Wu, J.-G. Wu, M.-R. Yu, T.-K. Tsai, C.-T. Yeh, Promotive effect of CNT on Co<sub>3</sub>O<sub>4</sub>-SnO<sub>2</sub> in a semiconductor-type CO sensor working at room temperature. *Sens. Actuators. B. Chem.* **131**, 306–312 (2008)
  17. J.-K. Kim, H. Kim, S.H. Park, T. Jeong, M.J. Bae, Y.C. Kim, I. Han, D. Jung, S. Yu, Effect of a critical percolation threshold in purified short carbon nanotube-polymer/ZnS:Cu, Cl composite on electroluminescence. *Org. Electron.* **13**, 2959–2966 (2012)
  18. B.K. Grandhe, V.R. Bandi, K. Jang, S. Ramaprabhu, H.-S. Lee, D.-S. Shin, S.S. Yi, J.-H. Jeong, Multi wall carbon nanotubes assisted synthesis of YVO<sub>4</sub>:Eu<sup>3+</sup> nanocomposites for display device applications. *Compos. Part B. Eng.* **43**, 1192–1195 (2012)
  19. S.W. Kim, T. Kim, Y.S. Kim, H.S. Choi, H.J. Lim, S.J. Yang, C.R. Park, Surface modifications for the effective dispersion of carbon nanotubes in solvents and polymers. *Carbon* **50**, 3–33 (2012)
  20. J. Yan, Z. Fan, L. Zhi, Functionalized carbon nanotubes and their enhanced polymers, in *Polymer Science: A Comprehensive Reference*, ed. by K. Matyjaszewski, M. Möller (Elsevier, Amsterdam, 2012), pp. 1–8
  21. D. Tasis, J. Mikroyannidis, V. Karoutsos, C. Galiotis, K. Papangelis, Single-walled carbon nanotubes decorated with a pyrene-fluorenevinylene conjugate. *Nanotechnology* **20**, 135606 (2009)
  22. S.A. Ntim, O. Sae-Khow, F.A. Witzmann, S. Mitra, Effects of polymer wrapping and covalent functionalization on the stability of MWCNT in aqueous dispersions. *J. Colloid Interface Sci.* **355**, 383–388 (2011)
  23. A.R. Boccaccini, J. Choa, T. Subhani, C. Kaya, F. Kaya, Electrophoretic deposition of carbon nanotube–ceramic nanocomposites. *J. Eur. Ceram. Soc.* **30**, 1115–1129 (2010)
  24. B. Toboosung, P. Singjai, A flexible angle sensor made from MWNT/CuO/Cu<sub>2</sub>O nanocomposite films deposited by an electrophoretic co-deposition process. *J. Alloys Compd.* **533**, 62–66 (2012)
  25. Y.C. Fan, Y.M. Liu, Y.C. Chen, Y. Sung, M.D. Ger, Carbon nanotube field emission cathodes fabricated with chemical displacement plating. *Appl. Surf. Sci.* **255**, 7753–7758 (2009)
  26. C.K. Lin, C.H. Wu, C.Y. Tsai, C.Y. Chen, S.C. Wang, Pseudo capacitive performance of hybrid manganese oxide films with multiwalled-CNT additions. *Surf. Coat. Technol.* **205**, 1595–1598 (2010)
  27. C.-C. Kao, Y.-C. Liu, Intense green emission of ZnS:Cu, Al phosphor obtained by using diode structure of carbon nano-tubes field emission display. *Mater. Chem. Phys.* **115**, 463–466 (2009)
  28. G. Chen, L. Zhang, H. Ma, N. Yao, B. Zhang, Carbon nanotubes cathode of field emission lamp prepared by electrophoretic deposition. *Energy Procedia* **16**, 240–243 (2012)
  29. M.C. Schausten, D. Meng, R. Telle, A.R. Boccaccini, Electrophoretic deposition of carbon nanotubes and bioactive glass particles for bioactive composite coatings. *Ceram. Int.* **36**, 307–312 (2010)
  30. L. Besra, M. Liu, A review on fundamentals and applications of electrophoretic deposition (EPD). *Prog. Mater. Sci.* **52**, 1–61 (2007)
  31. A.R. Boccaccini, J. Cho, J.A. Roether, B.J.C. Thomas, E.J. Minay, M.S.P. Shaffer, Review electrophoretic deposition of carbon nanotubes. *Carbon N. Y.* **44**, 3149–3160 (2006)
  32. B. Ferrari, R. Moreno, EPD kinetics: a review. *J. Eur. Ceram. Soc.* **30**, 1069–1078 (2010)
  33. I. Corni, M.P. Ryan, A.R. Boccaccini, Electrophoretic deposition: from traditional ceramics to nanotechnology. *J. Eur. Ceram. Soc.* **28**, 1353–1367 (2008)
  34. A. Naeimi, A.M. Arabi, A.R. Gardeshzadeh, M. ShafieeAfarani, Study of electrophoretic deposition of ZnS:Ag/CNT composites for luminescent applications. *J. Mater. Sci.: Mater. Electron.* **25**, 1575–1582 (2014)
  35. K. Balamurugan, P. Baskar, R. Mahesh Kumar, S. Das, V. Subramanian, Interaction of carbon nanotube with ethylene glycol–water binary mixture: a molecular dynamics and density functional theory investigation. *J. Phys. Chem. C* **116**, 4365–4373 (2012)
  36. T.-T. Chen, C.-H. Yang, W.-T. Tsai, In-situ synchrotron X-ray diffraction study on the dehydrogenation behavior of NaAlH<sub>4</sub> modified by multi-walled carbon nanotubes. *Int. J. Hydrog. Energy* **37**, 14285–14291 (2012)
  37. L. Liang, Y. He, H. Song, X. Yang, X. Cai, C.Y. Xiong, Y. Li, Effect of hydration pretreatment on tunnel etching behaviour of aluminium foil. *Corros. Sci.* **70**, 180–187 (2013)

38. Z. Hu, B. Ma, S. Liu, M. Narayanan, U. Balachandran, Ceramic dielectric film capacitors fabricated on aluminum foils by chemical solution deposition. *Mater. Res. Bull.* **52**, 189–193 (2014)
39. X. Qi, G. Poernomo, K. Wang, Y. Chen, M.B. Chan-Park, R. Xu, M.W. Chang, Covalent immobilization of nisin on multi-walled carbon nanotubes: superior antimicrobial and anti-biofilm properties. *Nanoscale* **3**, 1874–1880 (2011)
40. J. Navamani, R. Palanisamy, R. Gurusamy, M. Ramasamy, S. Arumugam, Development of nanoprobe for the determination of blood cholesterol. *J. Biosens. Bioelectron.* **3**, 1–8 (2012)
41. G. Ghosh, M.K. Naskar, Synthesis and characterization of PVP-encapsulated ZnS nanoparticles. *Opt. Mater.* **28**, 1047–1053 (2006)
42. S. Kuche Loghmani, M. Farrokhi-Rad, T. Shahrabi, Effect of polyethyleneglycol on the electrophoretic deposition of hydroxyapatite nanoparticles in isopropanol. *Ceram. Int.* **39**, 7043–7051 (2013)
43. K.-T. Lau, C.C. Sorrell, Electrophoretic mobilities of dissolved polyelectrolyte charging agent and suspended non-colloidal titanium during electrophoretic deposition. *Mater. Sci. Eng. B* **176**, 369–381 (2011)
44. R.B. Pandey, Polymer interface changes in electrophoretic deposition. *Prog. Org. Coat* **47**, 324–330 (2003)
45. K. Tada, M. Onoda, Preparation and application of nanostructured conjugated polymer film by electrophoretic deposition. *Thin Solid Films* **438–439**, 365–368 (2003)
46. Z. Rui, L. Yingbo, Synthesis and characterization of high-quality colloidal Mn<sup>2+</sup>-doped ZnS nanoparticles. *Opt. Mater.* **34**, 1788–1794 (2012)
47. Y. Chen, B. Wang, S. Dong, Y. Wang, Y. Liu, Rectangular microscale carbon tubes with protuberant wall for high-rate electrochemical capacitors. *Electrochim. Acta* **80**, 34–40 (2012)
48. K. Manzoor, S.R. Vadera, Energy transfer from organic surface adsorbate-polyvinyl pyrrolidone molecules to luminescent centers in ZnS nano crystals. *Solid State Commun.* **129**, 469–473 (2004)